American Mineralogist, Volume 86, pages 690–696, 2001

Single-crystal in situ high-temperature structural investigation on strontium feldspar

PIERA BENNA* AND EMILIANO BRUNO

Dipartimento di Scienze Mineralogiche e Petrologiche, Via Valperga Caluso 35, I-10125 Torino; and Centro di Studi sulla Geodinamica delle Catene Collisionali (C.N.R.), Via Accademia delle Scienze 5, I-10123 Torino, Italy

ABSTRACT

A single crystal of ordered strontium feldspar ($SrAl_2Si_2O_8$) was used for in situ X-ray intensity data collection at T = 20, 160, 330, 510, and 670 °C. The crystal was synthesized from the melt and thermally treated at T = 1450 °C for 146 h (a = 8.379, b = 12.963, c = 14.245 Å, β = 115.46 °, V = 1397.0 Å^3; Q_{od} = 0.82). At room temperature 1517 reflections of *a*-type and 988 reflections of *b*-type with $F_o \geq 2\sigma(F_o)$ were observed with R = 4.0% for refinement in space group *I*2/*c*. The dimensions of the tetrahedra do not change significantly with increasing temperature implying that the Al-Si configuration remains unchanged throughout the experimentally investigated temperature range. The Sr-coordination polyhedron expands regularly with temperature. The linear coefficient of volume expansion ($\alpha_v = 1.69 \times 10^{-5}$ /°C) is close to that observed for the other feldspars. The thermal expansion ellipsoid shows a remarkable anisotropy and the main expansion occurs close to *a**, as observed in the other monoclinic K-, Ba-, and Pb-feldspars. The variation along *a** is related to the flexing of the double-crankshaft chains in response to the expansion of the Sr-polyhedron. As in Pb-feldspar, a progressive displacement of the non-tetrahedral cation towards the *c*-glide plane with increasing temperature is observed. However, in Sr-feldspar, the temperature increase does not cause the atoms of the M polyhedron to approach *C*2/*m* symmetry. These results suggest that the atoms of the Sr-polyhedron retain *I*2/*c* symmetry at elevated temperatures and the Sr-polyhedron does not assume a configuration that may significantly favor Al-Si disorder.

INTRODUCTION

Few works concerning high-temperature in-situ structural investigations on feldspars have been reported, except for high and low albite (Prewitt et al. 1976; Winter et al. 1977), anorthite (Czank 1973; Foit and Peacor 1973; Ghose et al. 1993) and sanidine (Ohashi and Finger 1974, 1975; Kimata et al. 1996). Recently, a high-temperature single-crystal investigation on Pb-feldspar ($PbAl_2Si_2O_8$) was performed by Benna et al. (1999).

In the present work, Sr-feldspar ($SrAl_2Si_2O_8$) was investigated in order to contribute to the study of the thermal behaviour of monoclinic feldspars. In particular, the structural evolution with temperature in Sr-feldspar is compared with the modifications recently observed in Pb-feldspar by Benna et al. (1999).

The structure of partially ordered Sr-feldspar (space group *I*2/*c*) was determined by Chiari et al. (1975). It was experimentally demonstrated (Benna et al. 1995) that the ordered Al-Si configuration (Q_{od} = 0.86) is the equilibrium state for Sr-feldspar, at least up to T = 1450 °C. The metastable disordered configuration was observed in Sr-feldspar crystallized from the melt in very short times (Q_{od} = 0) and refined in space group *C*2/*m* by Benna et al. (1995). Isothermal annealing of the disordered feldspar at T = 1350 and 1450 °C caused evolution towards greater Al-Si order. The change in space group from *C*2/*m* to *I*2/*c* with progressive Al-Si ordering can be followed during thermal treatments of metastable disordered samples. This change in space group corresponds to a *zone boundary* phase transition inducing the appearance of *b*-type ($h + k$ = odd, l = odd) superstructure reflections, that increase in intensity with increasing order (Carpenter et al. 1990).

Benna et al. (1996) synthesized Pb-feldspar in both ordered and disordered configurations. Disordered Pb-feldspar (space group *C*2/*m*) has a "split Pb-site configuration," while ordered Pb-feldspar retains space group *I*2/*c*, similar to that of Sr-feldspar. A significant distortion of the Pb-coordination polyhedron, in comparison with the Sr-polyhedron in Sr-feldspar, is observed, but the general features of Sr- and Pb-feldspars are similar, in both the ordered and the disordered forms. For Pb-feldspar, isothermal treatments of disordered crystals have shown a similar evolution towards higher degrees of ordering (Tribaudino et al. 1998). Treatment temperatures required to achieve ordering were significantly lower than those needed for Sr-feldspar. Tribaudino et al. (1998) showed that the transition from the ordered to the disordered configuration in Pb-feldspar can be experimentally bracketed in the subsolidus, suggesting a T_c between 1150 and 1200 °C for the *I*2/*c*-*C*2/*m* phase transition induced by the Al-Si order-disorder process. The disordered Al-Si configuration is therefore an equilibrium configuration in the subsolidus for Pb-feldspar, while for Sr-feldspar the *I*2/*c*-*C*2/*m* phase transition, and consequently the

* E-mail: benna@dsmp.unito.it

disordered Al-Si configuration, has not yet been experimentally attained at equilibrium.

More recently, the in situ high-temperature structural investigations on ordered Pb-feldspar have shown significant changes in the Pb-coordination polyhedron with an increase in temperature (Benna et al. 1999). In particular, the progressive approach of the Pb cation to the *c*-glide plane at high-temperature suggests that, near the melting temperature, the Pb-polyhedron could attain a more regular configuration which may favor Al-Si disorder. A significant correlation between the configuration of the non-tetrahedral cation and the degree of Al-Si order may exist, and so a comparison between the results obtained for Pb-feldspar and the in-situ thermal behavior of ordered Sr-feldspar seems promising.

Experimental method

The starting materials were gels of stoichiometric $SrAl_2Si_2O_8$ composition prepared according to the method of Biggar and O'Hara (1969). Single crystals of Sr-feldspar were obtained by cooling a gel melted by oxy-acetylene flame. Samples were then thermally treated at $T = 1450$ °C for 146 h. Annealing was performed in an electric furnace (SiC resistance, Pt-PtRh 10% thermocouple) using unsealed tubes of platinum with subsequent quenching in air. Synthesis products were first examined by X-ray powder diffraction (Guinier camera, Cu$K\alpha$ radiation, = 1.54178 Å) and then by electron microscopy. The crystal chosen for data collection ($0.15 \times 0.14 \times 0.10$ mm) was fixed to a quartz glass fiber using GA-100 high-temperature cement. Single-crystal X-ray diffraction was performed in situ at T = 20, 160, 330, 510, and 670 °C. Intensities were collected with a Siemens *P*4 four-circle diffractometer, using graphite-monochromatized Mo$K\alpha$ radiation ($\lambda = 0.71073$ Å) in the θ-2θ scan mode. An A.E.T. thermal attachment (Pt-PtRh 10% thermocouple) using a stream of hot N_2 gas was employed for high-temperature single-crystal diffraction (Argoud and Capponi 1984). Diffractometer angles for same set of 40 reflections were collected for unit-cell parameter refinements at intervals of about 80 °C. Reflections up to $2\theta = 70°$, including two sets of equivalent reflections ($h, \pm k, \pm l$) were measured with a variable scanning speed (2.4–30 °/min). An empirical absorption correction based on the ψ-scan method (North et al. 1968) at room temperature was used for all data sets since at higher temperatures the heating attachment prevented measurement of the required ψ-scans. Data were corrected for background and Lorentz-polarization effects using the SHELXTL-Plus 1990 system. A weighting scheme was used for the data only at the end of refinement cycles. In all data sets *a* and *b* reflections (*a*-type: $h + k$ = even, l = even, following Bown and Gay 1958) were found and space group *I*2/*c* was assumed. Reflections with $F_o \geq 2\sigma(F_o)$ were regarded as observed and used for the refinements.

Unit-cell parameters, refinement data, atomic fractional coordinates and displacement parameters are given in Tables 1 and 2. Relevant interatomic distances are listed in Tables 3 and 4. The macroscopic order parameter Q_{od}, calculated from the room temperature data using the calibration of Angel et al. (1990), is 0. 82. Table 5[1] contains the observed and calculated structure factors.

Results and discussion

Unit-cell parameters vary linearly with temperature. The most significant expansion is observed in *a* and *c* (Fig. 1), while the increase in *b* is rather small. A slight decrease in β is also observed. Thermal expansion of the unit-cell is similar to that observed in monoclinic feldspars (Oehlschlegel et al. 1974; Henderson and Ellis 1976; Henderson 1984; Ribbe 1994). The linear coefficient of volume expansion ($\alpha_V = 1.69 \times 10^{-5}$ /°C) is close to that of Pb-feldspar (1.26×10^{-5} /°C, Benna et al. 1999). In Table 6 the three principal coefficients of the thermal strain are listed, calculated as in Ohashi (1982).

With increasing temperature the *y*-coordinate of the Sr atom changes from $y = 0.0021$ at room temperature to $y = 0.0013$ at $T = 670$ °C (Fig. 2), so that the Sr atom progressively approaches the *c*-glide plane located at $y = 0$. The average T-O bond lengths, and therefore the Al Si site occupancies are not significantly changed at high-temperature, at least up to $T = 670$ °C (Table 3). The Al-Si distribution remains nearly unchanged through-

[1]For a copy of Table 5, Document AM-01-065, contact the Business Office of the Mineralogical Society of America (see inside front cover of recent issue) for price information. Deposit items may also be available on the *American Mineralogist* web site at http://www.minsocam.org.

Table 1. Single-crystal data at different temperatures (e.s.d. in brackets)

T (°C)	20	160	330	510	670
a (Å)	8.379(3)	8.392(3)	8.399(3)	8.414(3)	8.428(3)
b (Å)	12.963(4)	12.967(3)	12.963(4)	12.970(4)	12.975(4)
c (Å)	14.245(3)	14.260(3)	14.266(4)	14.280(3)	14.291(3)
β (°)	115.46(2)	115.43(2)	115.39(2)	115.34(2)	115.34(2)
V (Å^3)	1397.0	1401.4	1403.2	1408.4	1412.4
μ (mm^{-1})	8.33	8.30	8.29	8.26	8.23
Refl. measured	7020	6175	6144	6145	6177
Unique refl.	3063	2838	2832	2834	2842
Refl. observed $F_o \geq 2\sigma(F_o)$	2505	2159	2023	1900	1820
Refl. *b*-type	988	819	740	652	611
No. refl. *b* / No. refl. *a*	0.651	0.611	0.577	0.522	0.505
$\Sigma F^2_{o(b)}/\Sigma F^2_{o(a)}$ $F_o \geq 2\sigma(F_o)$	0.028	0.027	0.026	0.025	0.025
R	0.040	0.053	0.061	0.067	0.077
wR^2	0.082	0.106	0.120	0.125	0.137
Goodness of fit	1.11	1.13	1.14	1.17	1.18

Note: $w = 1/[\sigma^2(F_o^2) + (0.1P)^2]$, where $P = (F_o^2 + 2F_c^2)/3$.

TABLE 2. Atomic fractional coordinates (×10⁴), equivalent isotropic and anisotropic displacement coefficients (Å² × 10³)

Site	*x*	*y*	*z*	U_{eq}	U_{11}	U_{22}	U_{33}	U_{12}	U_{13}	U_{23}
					***T* = 20 °C**					
Sr	2691(1)	–21(1)	656(1)	16(0)	7(0)	24(0)	16(0)	–0(0)	2(0)	–2(0)
$T_1(0)$	70(1)	1747(1)	1086(1)	7(0)	6(0)	9(0)	5(0)	–2(0)	2(0)	–0(0)
$T_1(z)$	32(1)	1776(1)	6162(1)	7(0)	6(0)	9(0)	5(0)	–2(0)	2(0)	–0(0)
$T_2(0)$	6939(1)	1203(1)	1705(1)	6(0)	4(0)	7(0)	5(0)	–0(0)	1(0)	0(0)
$T_2(z)$	6854(1)	1133(1)	6716(1)	7(0)	5(0)	7(0)	6(0)	–0(0)	1(0)	–0(0)
$O_A(1)$	44(3)	1292(1)	2(1)	11(0)	12(1)	15(1)	5(1)	0(1)	3(1)	0(1)
$O_A(2)$	5914(2)	–1(1)	1428(1)	10(0)	6(1)	8(1)	14(1)	–0(1)	1(1)	0(1)
$O_B(0)$	8280(3)	1264(2)	1066(1)	14(0)	11(1)	18(1)	16(1)	–5(1)	8(1)	–3(1)
$O_B(z)$	8089(3)	1267(2)	6111(1)	14(0)	11(1)	17(1)	15(1)	–3(1)	7(1)	1(1)
$O_C(0)$	134(3)	2981(1)	1184(1)	14(0)	12(1)	13(1)	14(1)	–5(1)	4(1)	–1(1)
$O_C(z)$	182(3)	3091(1)	6304(2)	13(0)	11(1)	11(1)	16(1)	–5(1)	5(1)	–3(1)
$O_D(0)$	1876(3)	1247(2)	1961(1)	15(0)	12(1)	20(1)	8(1)	1(1)	0(1)	2(1)
$O_D(z)$	1975(3)	1188(2)	7037(1)	13(0)	11(1)	17(1)	8(1)	1(1)	–0(1)	1(1)
					***T* = 160 °C**					
Sr	2707(1)	–18(1)	657(1)	25(0)	11(0)	35(0)	27(0)	–0(0)	4(0)	–3(0)
$T_1(0)$	67(1)	1753(1)	1085(1)	11(0)	10(1)	13(0)	9(0)	–3(0)	4(0)	–1(0)
$T_1(z)$	36(2)	1781(1)	6162(1)	10(0)	9(1)	13(0)	9(0)	–3(0)	3(0)	–1(0)
$T_2(0)$	6949(2)	1204(1)	1708(1)	10(0)	8(1)	11(1)	10(0)	–1(0)	3(0)	–0(0)
$T_2(z)$	6864(1)	1134(1)	6718(1)	10(0)	7(0)	10(0)	12(0)	–1(0)	3(0)	–0(0)
$O_A(1)$	43(5)	1296(2)	4(2)	16(0)	19(1)	21(1)	10(1)	–2(1)	7(1)	–3(1)
$O_A(2)$	5937(3)	–2(2)	1430(2)	17(0)	10(1)	11(1)	26(1)	1(1)	5(1)	–1(1)
$O_B(0)$	8280(4)	1270(3)	1068(3)	22(1)	19(2)	26(2)	25(1)	–6(1)	14(1)	–3(1)
$O_B(z)$	8105(4)	1276(3)	6116(3)	22(1)	17(2)	25(2)	29(2)	–5(1)	14(1)	2(1)
$O_C(0)$	138(4)	2987(2)	1187(2)	21(1)	19(2)	16(1)	23(1)	–6(1)	6(1)	–2(1)
$O_C(z)$	198(4)	3096(2)	6308(3)	21(1)	16(2)	17(1)	28(1)	–8(1)	7(1)	–5(1)
$O_D(0)$	1862(5)	1255(3)	1964(2)	24(1)	20(2)	30(2)	15(1)	3(1)	2(1)	3(1)
$O_D(z)$	1963(4)	1191(3)	7032(2)	21(1)	15(2)	26(2)	14(1)	1(1)	–1(1)	2(1)
					***T* = 330 °C**					
Sr	2722(1)	–16(1)	658(1)	35(0)	16(0)	46(0)	37(0)	–0(0)	5(0)	–3(0)
$T_1(0)$	72(2)	1759(1)	1086(1)	15(0)	14(1)	18(1)	13(0)	–4(0)	6(0)	–1(0)
$T_1(z)$	36(2)	1785(1)	6162(1)	15(0)	14(1)	17(1)	13(1)	–4(1)	6(1)	–1(0)
$T_2(0)$	6961(2)	1207(1)	1711(1)	14(0)	12(1)	14(1)	16(1)	–1(1)	4(1)	0(0)
$T_2(z)$	6877(2)	1136(1)	6722(1)	14(0)	11(1)	14(1)	16(1)	–2(0)	4(0)	–1(0)
$O_A(1)$	49(5)	1303(3)	8(3)	24(1)	30(2)	29(1)	13(1)	–4(2)	11(1)	–3(1)
$O_A(2)$	5955(4)	–3(3)	1432(3)	23(1)	13(1)	14(1)	36(2)	–1(2)	5(1)	–2(2)
$O_B(0)$	8282(5)	1278(3)	1070(3)	29(1)	25(2)	35(2)	34(2)	–10(2)	18(2)	–3(2)
$O_B(z)$	8107(5)	1284(3)	6117(3)	32(1)	25(2)	36(2)	42(2)	–7(2)	21(2)	2(2)
$O_C(0)$	136(5)	2990(3)	1184(3)	28(1)	24(2)	22(2)	31(2)	–7(1)	6(2)	–4(1)
$O_C(z)$	204(5)	3102(3)	6312(3)	28(1)	22(2)	19(2)	36(2)	–10(1)	7(2)	–6(1)
$O_D(0)$	1856(5)	1259(3)	1960(3)	32(1)	27(2)	41(2)	20(2)	5(2)	3(2)	7(1)
$O_D(z)$	1959(5)	1196(3)	7033(3)	29(1)	23(2)	33(2)	21(2)	2(2)	–0(2)	2(1)
					***T* = 510 °C**					
Sr	2738(1)	–14(1)	659(1)	45(0)	21(0)	58(0)	47(0)	–0(0)	7(0)	–3(0)
$T_1(0)$	72(2)	1764(1)	1085(2)	19(0)	18(1)	23(1)	16(1)	–4(1)	7(1)	–1(1)
$T_1(z)$	39(2)	1789(1)	6162(1)	19(0)	19(1)	21(1)	17(1)	–5(1)	8(1)	–2(1)
$T_2(0)$	6972(2)	1211(1)	1714(1)	19(0)	14(1)	19(1)	20(1)	–2(1)	6(1)	–0(1)
$T_2(z)$	6886(2)	1137(1)	6723(1)	18(0)	14(1)	17(1)	21(1)	–1(1)	5(1)	–1(1)
$O_A(1)$	44(6)	1313(3)	6(3)	30(1)	38(2)	35(2)	18(1)	0(2)	14(1)	–2(2)
$O_A(2)$	5977(5)	–2(3)	1434(3)	30(1)	18(2)	18(1)	47(2)	–0(2)	6(1)	–1(2)
$O_B(0)$	8282(6)	1292(4)	1069(3)	38(1)	31(2)	47(3)	43(2)	–8(2)	23(2)	–2(2)
$O_B(z)$	8118(6)	1291(4)	6120(4)	40(1)	31(2)	47(3)	50(3)	–11(2)	25(2)	1(2)
$O_C(0)$	141(6)	3001(3)	1186(3)	34(1)	30(3)	28(3)	39(2)	–9(2)	10(2)	–4(2)
$O_C(z)$	216(6)	3104(3)	6321(4)	35(1)	27(3)	26(2)	46(2)	–12(2)	10(2)	–8(2)
$O_D(0)$	1843(6)	1262(4)	1959(3)	41(1)	35(3)	54(3)	23(2)	6(2)	2(2)	5(2)
$O_D(z)$	1960(6)	1199(4)	7034(3)	37(1)	30(2)	43(3)	24(2)	5(2)	-0(2)	2(2)
					***T* = 670 °C**					
Sr	2746(1)	–13(1)	660(1)	50(0)	22(0)	66(1)	54(0)	0(1)	8(0)	–4(1)
$T_1(0)$	72(2)	1770(2)	1086(1)	21(1)	20(1)	25(1)	19(1)	–5(1)	9(1)	–1(1)
$T_1(z)$	39(3)	1790(2)	6164(1)	22(0)	21(1)	24(1)	19(1)	–5(1)	8(1)	–1(1)
$T_2(0)$	6975(3)	1213(2)	1715(2)	21(0)	17(1)	20(1)	24(1)	–2(1)	7(1)	–2(1)
$T_2(z)$	6893(2)	1136(1)	6725(1)	20(0)	15(1)	19(1)	23(1)	–1(1)	5(1)	0(1)
$O_A(1)$	52(8)	1319(4)	10(4)	33(1)	38(2)	44(2)	21(2)	–7(3)	15(2)	–8(2)
$O_A(2)$	5995(6)	–5(4)	1437(4)	34(1)	22(2)	19(2)	54(2)	–0(2)	9(2)	–3(3)
$O_B(0)$	8294(7)	1305(5)	1068(4)	42(1)	36(3)	48(3)	52(3)	–16(3)	30(3)	–6(3)
$O_B(z)$	8107(7)	1281(5)	6122(5)	44(1)	28(3)	54(4)	56(3)	–9(3)	24(3)	5(3)
$O_C(0)$	139(7)	3006(4)	1186(4)	37(1)	32(3)	30(3)	44(3)	–9(2)	10(2)	–6(2)
$O_C(z)$	229(7)	3106(4)	6325(5)	40(1)	31(3)	30(3)	54(3)	–16(2)	12(3)	–7(2)
$O_D(0)$	1838(8)	1265(5)	1964(4)	46(1)	38(3)	59(4)	27(2)	4(3)	2(3)	5(3)
$O_D(z)$	1963(7)	1203(5)	7027(4)	40(1)	31(3)	49(3)	30(2)	8(3)	2(2)	3(2)

Note: U_{eq} defined as one third of the trace of the orthogonalized U_{ij} tensor. The anisotropic displacement exponent takes the form: $-2\pi^2 (h^2a^{*2}U_{11} + k^2b^{*2}U_{22} + l^2c^{*2}U_{33} + 2hka^*b^*U_{12} + 2hla^*c^*U_{13} + 2klb^*c^*U_{23})$.

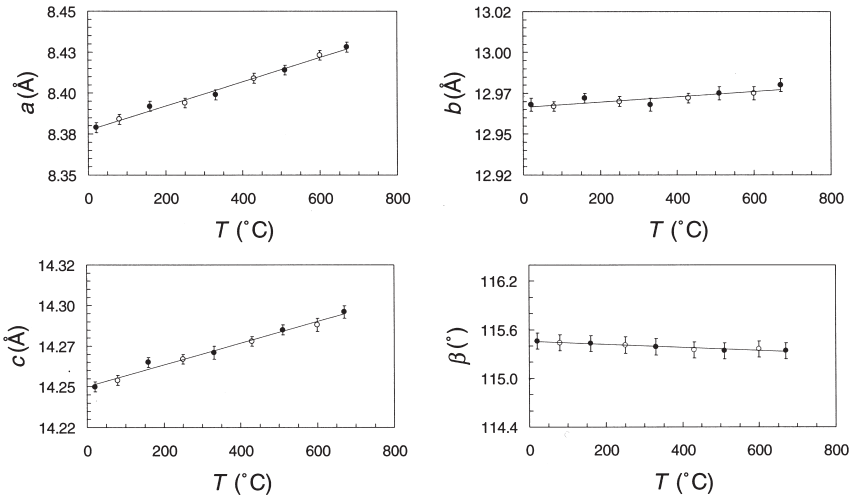

FIGURE 1. Lattice parameters vs. *T*. Open circles: unit-cell parameter refinements. Full circles: unit-cell parameter and crystal structure refinements. Bars indicate esd.

TABLE 3. T-O bond lengths (Å)

T (°C)	20	160	330	510	670
$T_1(0)$-$O_A(1)$	1.644(2)	1.643(3)	1.641(3)	1.639(4)	1.638(5)
$T_1(0)$-$O_B(0)$	1.614(2)	1.617(3)	1.619(4)	1.616(4)	1.606(5)
$T_1(0)$-$O_C(0)$	1.604(2)	1.606(3)	1.600(4)	1.610(4)	1.609(6)
$T_1(0)$-$O_D(0)$	1.626(2)	1.623(4)	1.618(4)	1.615(5)	1.619(6)
Mean	1.622	1.622	1.620	1.620	1.618
$T_1(z)$-$O_A(1)$	1.748(2)	1.751(3)	1.755(3)	1.752(4)	1.756(5)
$T_1(z)$-$O_B(z)$	1.729(2)	1.723(3)	1.722(4)	1.718(4)	1.734(5)
$T_1(z)$-$O_C(z)$	1.714(2)	1.716(3)	1.719(4)	1.718(4)	1.721(6)
$T_1(z)$-$O_D(z)$	1.744(2)	1.737(3)	1.736(4)	1.740(5)	1.737(5)
Mean	1.734	1.732	1.733	1.732	1.737
$T_2(0)$-$O_A(2)$	1.742(2)	1.743(3)	1.745(4)	1.746(4)	1.748(5)
$T_2(0)$-$O_B(0)$	1.726(2)	1.721(3)	1.716(4)	1.716(4)	1.727(5)
$T_2(0)$-$O_C(0)$	1.730(2)	1.730(3)	1.735(4)	1.731(5)	1.729(6)
$T_2(0)$-$O_D(0)$	1.726(2)	1.722(3)	1.723(4)	1.724(4)	1.718(6)
Mean	1.731	1.729	1.730	1.729	1.731
$T_2(z)$-$O_A(2)$	1.632(2)	1.629(3)	1.628(4)	1.628(4)	1.621(5)
$T_2(z)$-$O_B(z)$	1.616(2)	1.620(3)	1.616(4)	1.618(4)	1.607(5)
$T_2(z)$-$O_C(z)$	1.616(2)	1.610(3)	1.609(4)	1.608(4)	1.605(5)
$T_2(z)$-$O_D(z)$	1.620(2)	1.626(3)	1.622(4)	1.620(4)	1.626(6)
Mean	1.621	1.621	1.619	1.619	1.615

Note: bond lengths were not corrected for vibrational motion.

TABLE 4. Sr-O bond lengths (Å)

T (°C)	20	160	330	510	670
Sr-$O_A(1)$	2.646(2)	2.663(3)	2.684(4)	2.705(4)	2.723(5)
Sr-$O_A(1)$	2.628(2)	2.643(3)	2.653(4)	2.676(4)	2.683(6)
Sr-$O_A(2)$	2.439(2)	2.449(3)	2.454(3)	2.463(4)	2.476(4)
Sr-$O_B(0)$	2.749(2)	2.760(3)	2.771(4)	2.786(5)	2.798(6)
Sr-$O_B(z)$	2.851(2)	2.862(3)	2.869(4)	2.876(5)	2.872(6)
Sr-$O_C(0)$	3.229(2)	3.216(3)	3.205(4)	3.189(5)	3.181(6)
Sr-$O_C(z)$	3.090(2)	3.090(3)	3.082(4)	3.085(5)	3.089(6)
Sr-$O_D(0)$	2.778(2)	2.800(3)	2.806(4)	2.819(5)	2.833(6)
Sr-$O_D(z)$	2.746(7)	2.756(3)	2.770(4)	2.783(5)	2.782(6)

out the experimentally investigated temperature range. All the Sr-O bond lengths increase linearly with temperature (Table 4) except for Sr-OC distances, which slightly decrease. Hence, the Sr-coordination polyhedron regularly expands as indicated in Figure 3.

Increasing temperature induces a significant decrease in the intensity of *b* superlattice reflections, relative to the *a* sublattice reflections (Table 1), caused, in part, by the displacement of

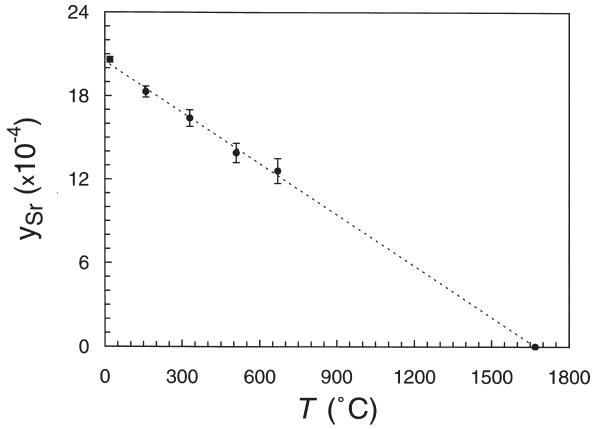

FIGURE 2. Absolute value of *y*-coordinate of the Sr site vs. *T*.

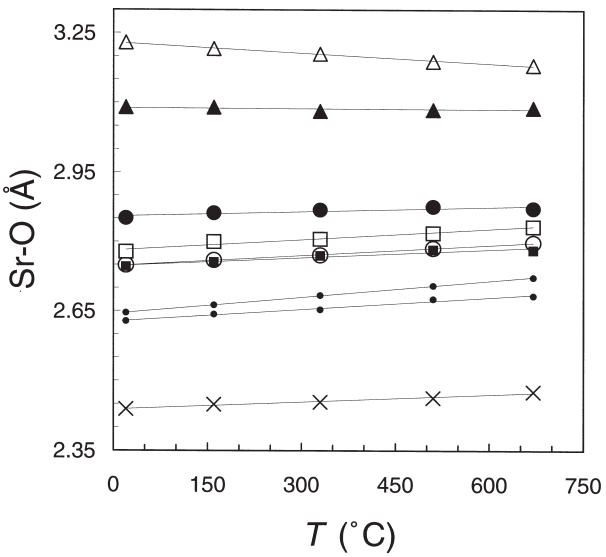

FIGURE 3. Sr-O distances vs. *T*. Points = OA1. Crosses = OA2. Circles = OB; triangles = OC; squares = OD; open symbol = 0; full symbol = *z*.

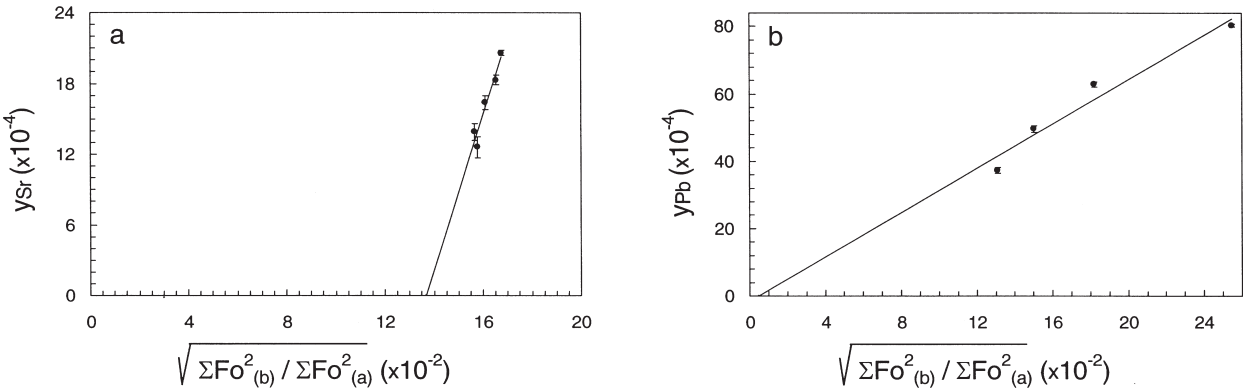

FIGURE 4. Absolute value of *y*-coordinate of the M site vs. $\sqrt{\Sigma F_o^2(b) / \Sigma F_o^2(a)}$ in (**a**) Sr-feldspar and (**b**) Pb-feldspar (Benna et al. 1999).

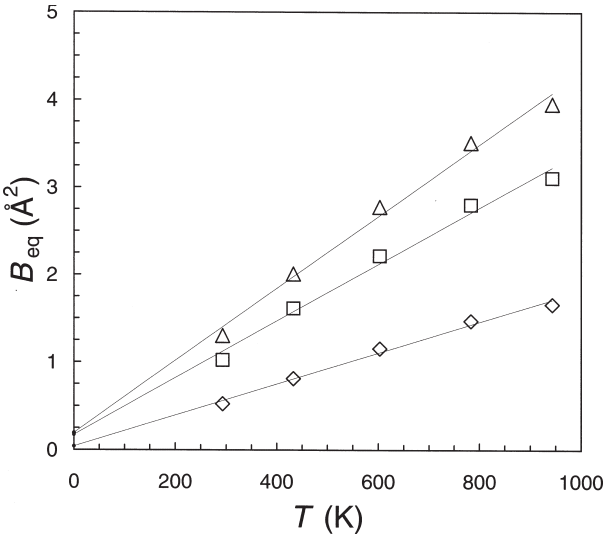

FIGURE 5. Equivalent isotropic displacement parameters B_{eq} vs. *T*. Triangles = Sr atom. Squares = O atoms. Diamonds = T atoms.

the Sr cation towards the glide plane. In Figure 4 the variation of the *y*-coordinate of the M site vs. $\sqrt{\Sigma F_o^2(b) / \Sigma F_o^2(a)}$ is reported for Sr- and Pb-feldspars. Figure 4a shows that, if we extrapolate y_{Sr} to zero, the calculated value of $\sqrt{\Sigma F_o^2(b) / \Sigma F_o^2(a)}$ is still very large (13.7×10^{-2}) indicating that the Sr contribution to the intensity of *b* reflections is small and that the alumino-silicate framework contribution (Al-Si order) remains significant over the investigated temperature range. Indeed in Pb-feldspar (Fig. 4b), if we extrapolate y_{Pb} to zero, the value of $\sqrt{\Sigma F_o^2(b) / \Sigma F_o^2(a)}$ also approaches zero, meaning that in Pb-feldspar the Pb contribution prevails and the intensity of *b* reflections is due mainly to a shift in the *y*-coordinate of the Pb atom (Benna et al. 1999).

In Figure 5 the isotropic equivalent displacement parameters (B_{eq}) for Sr, O, and T atoms as a function of temperature are plotted. An extrapolation of the higher temperature data to 0 K does not show the presence of a considerable residual, indicating a lack of positional disorder, unlike in Pb-feldspar, in which the positional disorder is significant.

TABLE 6. Principal axes and orientations of the strain ellipsoid (20–670 °C)

	Strain (×10⁻³)	Angle with		
		a	b	c
ε_1	6.9 (5)	32	90	83
ε_2	3.2 (3)	122	90	7
ε_3	0.9 (4)	90	0	90

Note: The reference state is at T = 20 °C.

Anisotropy of the strain tensor with temperature

In Sr-feldspar the thermal expansion ellipsoid shows a considerable anisotropy, the principal expansion (ε_1) occurring close to *a** (Table 6) as observed in the strains accompanying thermal expansion in monoclinic feldspars (Ohashi and Finger 1974, 1975; Henderson 1984; Kroll 1984; Brown et al. 1984). Moreover, if the magnitudes and orientations of the strains observed by Angel (1994) for sanidine with increasing pressure are considered, the most compressible direction corresponds to that of maximum thermal expansion with increasing temperature, although opposite in sign. Angel (1994) has recently emphasized the inverse behavior shown by monoclinic alkali feldspar under compression and thermal expansion.

The structural interpretation of the thermal expansion along *a** in feldspars has been discussed by several authors. Ohashi and Finger (1974, 1975), studying sanidine at high-temperature, correlate the tilts observed in the tetrahedral framework with lengthening of the M polyhedron along *a**. In a study of the thermal expansion in low albite, Winter et al. (1977) state that the cell expansion is principally controlled by adjustments of the alumino-silicate framework itself and that the Na cation plays a relatively "passive role." Brown et al. (1984) identify several different trends in the expansion behaviour of alkali feldspars. They suggest that the expansion is dominated by the alumino-silicate framework and not by expansion of the short M-O bonds of the non-tetrahedral cation. Angel (1994), examining the effects of compression of sanidine and anorthite, suggests that the tetrahedral framework controls compressibility in feldspars.

Comparison of the thermal expansion observed in Sr-, Pb-feldspars (Benna et al. 1999) and sanidine (Ohashi and Finger 1974, 1975) suggests a possible mechanism for structural

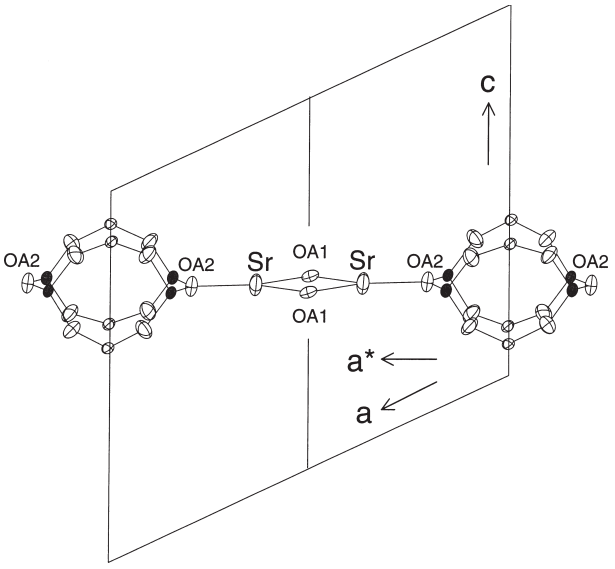

FIGURE 6. Partial [010] projection of the Sr-feldspar structure. Full ellipsoids: T2 atoms. Open ellipsoids without labels: T1, OB, and OD atoms. The Sr-Sr and the Sr-OA2 distances are almost parallel to a^*. The projection is slightly rotated to avoid overlapping of atoms.

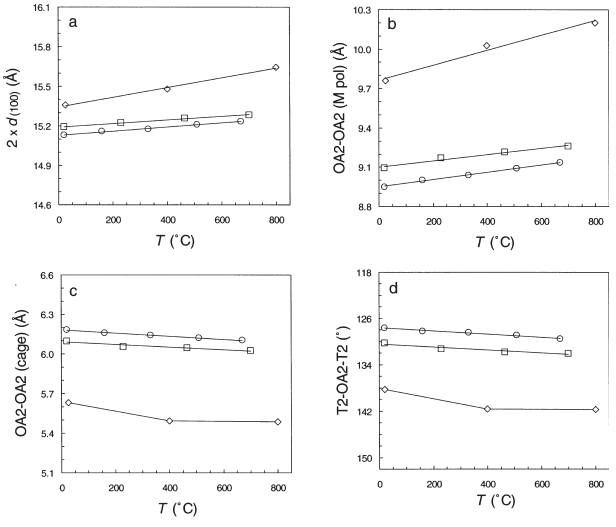

FIGURE 7. Relevant distances along a^* and T-O-T bond angles vs. T for Sr-feldspar (circles), Pb-feldspar (squares, Benna et al. 1999) and sanidine (diamonds, Ohashi and Finger 1974, 1975). (**a**) $2 \times d_{(100)}$; (**b**) OA2-OA2 (M pol): distance along the M polyhedron (see Fig. 6); (**c**) OA2-OA2 (cage): distance along the tetrahedral cage; (**d**) T2-OA2-T2 angle.

change as a function of temperature.

In Figure 6 a partial projection onto the (010) plane of the Sr-feldspar structure is depicted. The Sr-OA1 and Sr-OA2 bonds in the two Sr polyhedra, sharing the OA1-OA1 edge, and the two cages formed by tetrahedral four-fold rings are shown (Megaw 1974; Bruno and Facchinelli 1974; Kroll 1984). In Figure 7 the main structural features along a^* are reported as a function of temperature for Sr-, Pb-, and K-feldspars. Figure 7b shows the expansion, measured as the OA2-OA2 distance along a^*, in the two M polyhedra (see Fig. 6 in this work and Fig. 4 in Benna et al. 1999). Electrostatic repulsion between M cations, perpendicular to the shared edge OA1-OA1, can also contribute to an increase in the length of the OA2-OA2 distance (Megaw et al. 1962). The increase of this distance, observed in all three feldspars, is significantly larger than the unit-cell expansion along a^* (Fig. 7a), by doubling $d_{(100)}$. In contrast, if the OA2-OA2 distance across the tetrahedral cage is considered (Fig. 7c), then a reduction, mostly due to an increase of the T2-OA2-T2 bond angle, is observed. While the decrease in the OA2-OA2 (cage) distance along a^* is linear in Sr and Pb-feldspars, in sanidine this distance remains unchanged from 400 to 800 °C. Figure 7d shows that the T2-OA2-T2 angle increases linearly with temperature in Pb- and Sr-feldspars with a trend similar to that of the OA2-OA2 (cage) distance (Fig.7c). It is interesting to observe that for sanidine the T2-OA2-T2 angle remains constant from 400 to 800 °C, having reached its upper limit by T = 400 °C. To summarize, it appears that for Sr-, Pb-, and K-feldspars, the expansion of the M polyhedron causes a compression of the tetrahedral cage along a^*, due mainly to an increase in the T2-OA2-T2 angle.

On the basis of these results, we suggest that for monoclinic feldspars thermal expansion occurs mainly along a^* as a consequence of the flexing of the double-crankshaft chains in response to an expansion of the M polyhedron in the same direction.

Evolution of Sr-coordination polyhedron with temperature

As shown previously, in the temperature range 20–670 °C the Sr atom moves towards the c-glide plane with increasing temperature. The trend of the y_{Sr}-coordinate, extrapolated at high temperature in Figure 2, indicates that the y_{Sr} should go to zero at 1670 °C, surprisingly near the melting point of Sr-feldspar (T_{melt} ~ 1660 °C, Bambauer and Nager 1981). This suggests that the Sr atom could reach the symmetry plane, as already observed for Pb-feldspar (Benna et al. 1999, $y_{Pb} = 0$ at T = 1280 °C), at a temperature near the melting point (T_{melt} ~ 1300 °C). However, as the Sr atom approaches the glide plane, the O atoms of the Sr-polyhedron do not assume a configuration close to $C2/m$ symmetry, i.e., a configuration that may favor Al-Si disorder, as observed for Pb-feldspar (Tribaudino et al. 1998; Benna et al. 1999). We observe that, with increasing temperature, the separation between the OB(0)-OB(z), OC(0)-OC(z), and OD(0)-OD(z) atoms, related by the $c/2$ pseudotranslation (Foit and Peacor 1973), does not decrease. This has already been observed in Pb-feldspar, where the shift of the Pb atom away from the glide plane is larger than for Sr-feldspar and the bond lengths between Pb and O atoms, which are pseudosymmetric in $I2/c$, are progressively similar to one another with increasing temperature. For Sr-feldspar the configuration of the M polyhedron at elevated temperatures does not approach $C2/m$ symmetry (Table 4), as the displacement of the Sr atom away from the glide plane is very small. As observed by Newnham and Megaw (1960), in barium feldspar (celsian, space group $I2/c$) the position of the Ba cation on the glide plane at room temperature ($y_{Ba} = 0$) "is not a consequence of

the space group and is in a sense accidental." As for the Ba atom in celsian, the Sr cation in Sr-feldspar could "lie on a mirror plane which does not operate on the rest of the structure" (Newnham and Megaw 1960) as T_{melt} is approached.

In conclusion, the results obtained in this work by means of in situ high-temperature single-crystal X-ray diffraction suggest that in Sr-feldspar increasing temperature does not cause a progressive trend to *C*2/*m* symmetry in the atoms of the M polyhedron, as is observed for Pb-feldspar. An increase in temperature only causes the Sr atom to approach the glide plane, while the pseudosymmetrically related O atoms retain *I*2/*c* symmetry as observed at room temperature. Consequently, the configuration assumed by the M polyhedron at elevated temperatures does not seem to significantly favor Al-Si disorder.

ACKNOWLEDGMENTS

We thank two anonymous referees for critical reading and helpful suggestions. This work was supported by Project "Transformations, reactions, ordering in minerals" (MURST, Roma) and by C.S. Geodinamica Catene Collisionali (CNR, Torino).

REFERENCES CITED

Angel, R.J. (1994) Feldspars at high pressure. In I. Parsons, Ed., Feldspars and their reactions, p. 271–312. Kluwer, Dordrecht, The Netherlands.

Angel, R.J., Carpenter, M.A., and Finger, L.W. (1990) Structural variation associated with compositional variation and order-disorder behavior in anorthite-rich feldspar. American Mineralogist, 75, 150–162.

Argoud, R. and Capponi, J.J. (1984) Soufflette à haute température pour l'étude de monocristaux aux rayons X et aux neutrons jusqu'à 1400 K. Journal of Applied Crystallography, 17, 420–425.

Bambauer, H.U. and Nager, H.E. (1981) Gitterkonstanten und displazive Transformationen synthetischer Erdalkalifeldspäte. I. System $Ca[Al_2Si_2O_8]$-$Sr[Al_2Si_2O_8]$-$Ba[Al_2Si_2O_8]$. Neues Jahrbuch für Mineralogie Abhandlungen, 141, 225-239.

Benna, P., Tribaudino M., and Bruno E. (1995) Al-Si ordering in Sr-feldspar $SrAl_2Si_2O_8$: IR, TEM and single-crystal XRD evidences. Physics and Chemistry of Minerals, 22, 343–350.

———— (1996) The structure of ordered and disordered Pb-feldspar ($PbAl_2Si_2O_8$). American Mineralogist, 81, 1337–1343.

———— (1999) High temperature in situ structural investigation on Pb-feldspar. American Mineralogist, 84, 120–129.

Biggar, G.M. and O'Hara, M.J. (1969) A comparison of gel and glass starting materials for phase equilibrium studies. Mineralogical Magazine, 36, 198–205.

Bown, M.G. and Gay P. (1958) The reciprocal lattice geometry of the plagioclase feldspar structures. Zeitschrift für Kristallographie, 111, 1–14.

Brown, W.L., Openshaw, R.E., McMillan, P.F., and Henderson, C.M.B. (1984) A review of the expansion behavior of alkali feldspars: coupled variations in cell parameters and possible phase transitions. American Mineralogist, 69, 1058–1071.

Bruno, E. and Facchinelli, A. (1974) Correlations between the unit-cell dimensions and the chemical and structural parameters in plagioclases and in alkaline-earth feldspars. Bulletin de la Société française de Minéralogie et de Cristallographie, 97, 378–385.

Carpenter, M.A., Angel, R.J., and Finger, L.W. (1990) Calibration of Al/Si order variations in anorthite. Contributions to Mineralogy and Petrology, 104, 471–480.

Chiari, G., Calleri, M., Bruno, E., and Ribbe, P.H. (1975) The structure of partially disordered, synthetic Sr-feldspar. American Mineralogist, 60, 111–119.

Czank, M. (1973) Strukturuntersuchungen von Anorthit im Temperaturbereich von 20 °C bis 1430 °C. Dissertation. ETH Zürich.

Foit, F.F. and Peacor, J.R. (1973) The anorthite crystal structure at 410 and 830 °C. American Mineralogist, 58, 665–675.

Ghose, S., McMullan, R.K., and Weber, H.P. (1993) Neutron diffraction studies of the $P\bar{1}$-$I\bar{1}$ transition in anorthite ($CaAl_2Si_2O_8$), and the crystal structure of the body-centered phase at 514 K. Zeitschrift für Kristallographie, 204, 215–237.

Henderson, C.M.B. (1984) Thermal expansion of feldspars III. $RbGaSi_3O_8$-sanidine, Sr-feldspar and an ordered microcline-albite solid solution ($Or_{62.4}$, mol%). Natural Environment Research Council, Progress in Experimental Petrology, 25, 78–83, University Press, Cambridge, U.K.

Henderson, C.M.B. and Ellis J. (1976) Thermal expansion of synthetic alkali feldspars. Natural Environment Research Council, Progress in Experimental Petrology, 6, 55–59, Constable Ltd., Edinburgh, U.K.

Kimata, M., Shimizu, M., and Saito, S. (1996) High-temperature crystal structure of sanidine. Part II: The crystal structure of sanidine at 935 °C. European Journal of Mineralogy, 8, 15–24.

Kroll, H. (1984) Thermal expansion of alkali feldspars. In W.L. Brown, Ed., Feldspars and feldspathoids, p. 163–205. Reidel Publishing Company, Dordrecht, Holland.

Megaw, H.D. (1974) The architecture of the feldspars. In W.S. McKenzie and J. Zussman, Eds., The feldspars, p. 2–24. Manchester University Press, Manchester, U.K.

Megaw, H.D., Kempster, C.J.E., and Radoslovich, E.W. (1962) The structure of anorthite $CaAl_2Si_2O_8$. II. Description and discussion. Acta Crystallographica, 15, 1017–1035.

Newnham, R.E. and Megaw, H.D. (1960) The crystal structure of celsian (barium feldspar). Acta Crystallographica, 13, 303–313.

North, A.C.T., Phillips, D.C., and Mathews, F.S. (1968) A semi-empirical method of absorption correction. Acta Crystallographica, A24, 351–359.

Oehlschlegel, G., Kockel, A., and Biedl, A. (1974) Anisotrope Wärmedehnung und Mischkristallbildung einiger Verbindungen des ternären Systems BaO-Al_2O_3-SiO_2, II. Messungen an Strukturen mit dreidimensionaler Verknüpfung von $(Si,Al)O_4$-tetraedern und Modellvorstellungen uber deren Wärmedeh nungsanisotropie. Glastechnische Berichte, 47, 31–41.

Ohashi, Y. (1982) A program to calculate the strain tensor from two sets of unit-cell parameters. In R.M. Hazen and L.W. Finger, Eds., Comparative crystal chemistry, p. 92–102. Wiley, Chichester, U.K.

Ohashi, Y. and Finger, L.W. (1974) Refinement of the crystal structure of sanidine at 25° and 400 °C. Carnegie Institution of Washington Year Book 73, 539–544.

———(1975) An effect of temperature on the feldspar structure: crystal structure of sanidine at 800 °C. Carnegie Institution of Washington Year Book 74, 569–572.

Prewitt, C.T., Sueno, S., and Papike, J.J. (1976) The crystal structures of high albite and monalbite at high temperatures. American Mineralogist, 61, 1213–1225.

Ribbe, P.H. (1994) The crystal structures of the aluminum-silicate feldspars. In I. Parsons, Ed., Feldspars and their reactions, p. 1–49. Kluwer, Dordrecht, The Netherlands.

Tribaudino, M., Benna, P., and Bruno, E. (1998) Structural variations induced by thermal treatment in Pb-feldspar ($PbAl_2Si_2O_8$). American Mineralogist, 83, 159–166.

Winter, J.K., Ghose, S., and Okamura, F.P. (1977) A high-temperature study of the thermal expansion and the anisotropy of the sodium atom in low albite. American Mineralogist, 62, 921–931.

MANUSCRIPT RECEIVED AUGUST 16, 2000
MANUSCRIPT ACCEPTED JANUARY 31, 2001
MANUSCRIPT HANDLED BY JAMES W. DOWNS